Science Advances
AAAS

advances.sciencemag.org/cgi/content/full/4/10/eaau3489/DC1

Supplementary Materials for

Kinetic approach to superconductivity hidden behind a competing order

Hiroshi Oike*, Manabu Kamitani, Yoshinori Tokura, Fumitaka Kagawa*

*Corresponding author. Email: oike@ap.t.u-tokyo.ac.jp (H.O.); kagawa@ap.t.u-tokyo.ac.jp (F.K.)

Published 5 October 2018, *Sci. Adv.* **4**, eaau3489 (2018)
DOI: 10.1126/sciadv.aau3489

This PDF file includes:

Supplementary Materials and Methods

Quenching method

As a typical example of the electric-pulse rapid heating followed by rapid cooling, here we discuss the time profiles of the current and resistivity for the case that the quenching rate is not sufficiently high to kinetically avoid the formation of the charge order. Figure S1A,B displays the results of the sample #4 ($V \approx 180$ μm^3) on PEN substrate, in which the pulse amplitude was set at 19 mA and the rise, top-duration and fall times were set at 1, 1 and 3 s, respectively. The time-varying resistivity exhibits a complex profile because the melting and formation of the charge order are superimposed on the electric-pulse heating and subsequent cooling processes, respectively (fig. S1B). However, when the time-varying resistivity is plotted as a function of current (fig. S1C), the current-resistivity profile exhibits qualitatively similar behavior to the temperature-resistivity profile measured at a low temperature-sweep rate, 10^{-2} K s^{-1} (fig. S1D), indicating that the pulse application results in a rapid sweeping of the sample temperature, in this exemplary case, on the order of 10^2 K s^{-1}.

Given this, below, we explain the time-resistivity profile (fig. S1B) in greater detail. Before the pulse application, sample #4 on the PEN substrate was slowly cooled from 320 to 30 K, and thus, the initial state is the charge-ordered state (fig. S1D). To measure the resistivity of the electronic states before and after the pulse application, the pulse is offset by a low DC current, the value of which is one order of magnitude smaller than that of the pulse top (fig. S1A). During the pulse rising, the resistivity increases because of the Joule heating of the sample; it subsequently exhibits a sharp drop due to the melting of the charge-order. During the pulse top, the resistivity remained constant, indicating that the Joule heating is balanced with the thermal dissipation from the sample to the low-temperature substrate (see also fig. S3B). During the pulse falling, the Joule heating decreases accordingly; thus, in the course of the resistivity decrease, a sharp resistivity increase is observed due to the re-formation of the charge order. At the end of the fall time, the resistivity returns to the initial value, thus indicting that despite the intense Joule heating, the pulse application causes no appreciable damage to the sample.

Control of quenching rate

To control the quenching rate, we manipulated the fall time of the pulse. Figure S5A–D shows the time-varying current and resistivity during the pulse falling with various fall times. Here, we set the origin of the time at the beginning of the pulse fall, namely, at the moment when the sample temperature starts to decrease. The time profiles of the current and resistivity show a good correspondence, thus demonstrating that the quenching rate can be systematically tailored by manipulating the fall time. Whereas sample #4 ($V \approx 180$ μm^3) exhibits a peak structure in the time-resistivity profile because of the charge ordering upon cooling (figs. S1B and S5D), such a feature is not discernible in sample #3 ($V \approx 18$ μm^3) because the full development of the charge ordering is kinetically avoided by the combination of the sample miniaturization and rapid cooling. The highest cooling rate is achieved when the fall time is set to “zero” within the resolution of the function generator, and it is higher than 10^7 and 10^5 K s^{-1} for samples #3 (on the Si substrate) and #4 (on the PEN substrate), respectively (fig. S2). The difference in the highest cooling rate originates from that in thermal conductivity between Si and PEN substrates.

Numerical simulation

To examine whether the orders of the highest cooling rates estimated above are reasonable, we performed a finite element method using commercial software (COMSOL Multiphysics) and simulated the quenching procedure for an $IrTe_2$ thin plate on Si and PEN substrates. In the numerical simulation, we employed the geometry shown in fig. S3A,B, in which the $IrTe_2$ sample is modeled as a rectangular thin plate with dimensions of $16\times7\times0.2$ μm^3 and the substrate dimensions are $1\times1\times0.5$ mm^3. We set values of thermal conductivity κ, specific heat C_p, and resistivity ρ as follows

$\kappa = 10$ W m^{-1} s^{-1}, $C_p = 2\times10^6$ J K^{-1} m^{-3} and $\rho = 50$ $\mu\Omega$ cm for $IrTe_2$

$\kappa = 150$ W m^{-1} s^{-1}, $C_p = 2\times10^5$ J K^{-1} m^{-3} for Si substrate

$\kappa = 0.3$ W m^{-1} s^{-1}, $C_p = 2\times10^5$ J K^{-1} m^{-3} for PEN substrate

and the contact resistance of the current electrodes was set at 1.5 Ω

In reality, these parameters should vary with temperature, but for simplicity, we treated them as constants and performed an order-of-estimate calculation of the quenching rate. To model heat transfer with a thermal impedance from the sample to the substrate, we also assumed a contact layer between them. The thermal conductivity and heat capacity of the contact layer were treated as adjustable parameters, and they were determined to reproduce the experimental observations that the sample is heated to ~400 K by current applications of 160 and 19 mA for an $IrTe_2$ thin plate on Si and PEN substrates, respectively. In the simulation, the trapezoidal current pulse shown in fig. S3C was applied to the samples, with the same magnitude of current as that used in the experiments. Although the sample temperature is not uniform, we extracted the temperature at the center of the sample and plotted its time profile in fig. S3D. The quenching rate obtained in the simulation is 4×10^7 and 2×10^6 K s^{-1} for the sample on the Si and PEN substrates, respectively, and it is nearly the same order as that estimated from the experiments (fig. S2C,D). Thus, the numerical simulation supports the high quenching rate estimated from the experiment.

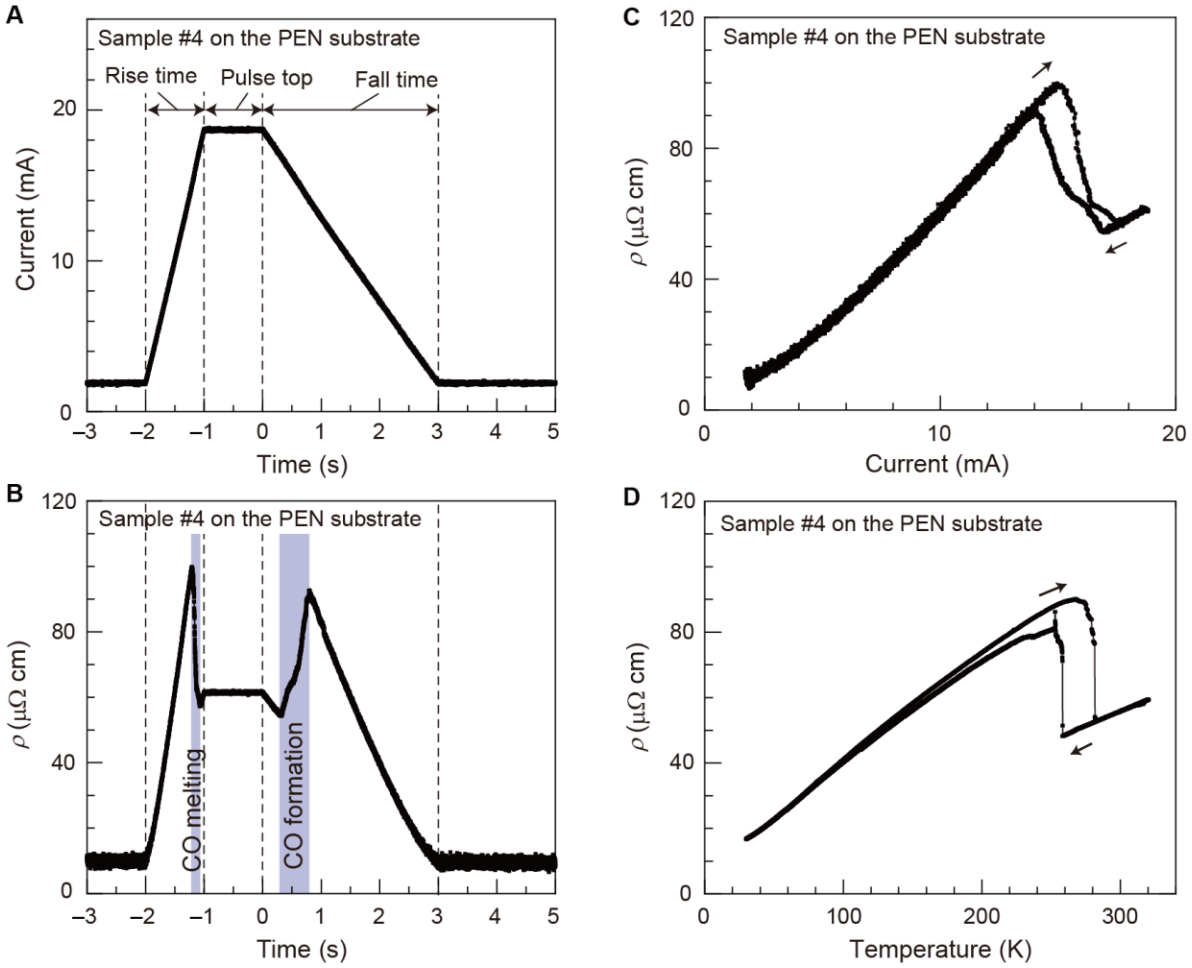

Fig. S1. Sample heating by a trapezoidal current-pulse application, followed by rapid cooling. (**A** and **B**) The time profiles of the applied current pulse (A) and the corresponding change in resistivity (B) in the $IrTe_2$ thin plate #4 ($V \approx 180$ μm^3) on PEN substrate. The vertical broken lines are visual guides, therein delimiting the time boundary between the pulse rising, pulse top, and pulse falling. CO in (B) denotes the charge order. The origin of the time is set at the beginning of the pulse fall. (**C**) The current-resistivity profile during the pulse application, extracted from (A) and (B). (**D**) The temperature-resistivity profile of the $IrTe_2$ thin plate #4, measured at a temperature-sweeping rate of 10^{-2} K s^{-1}.

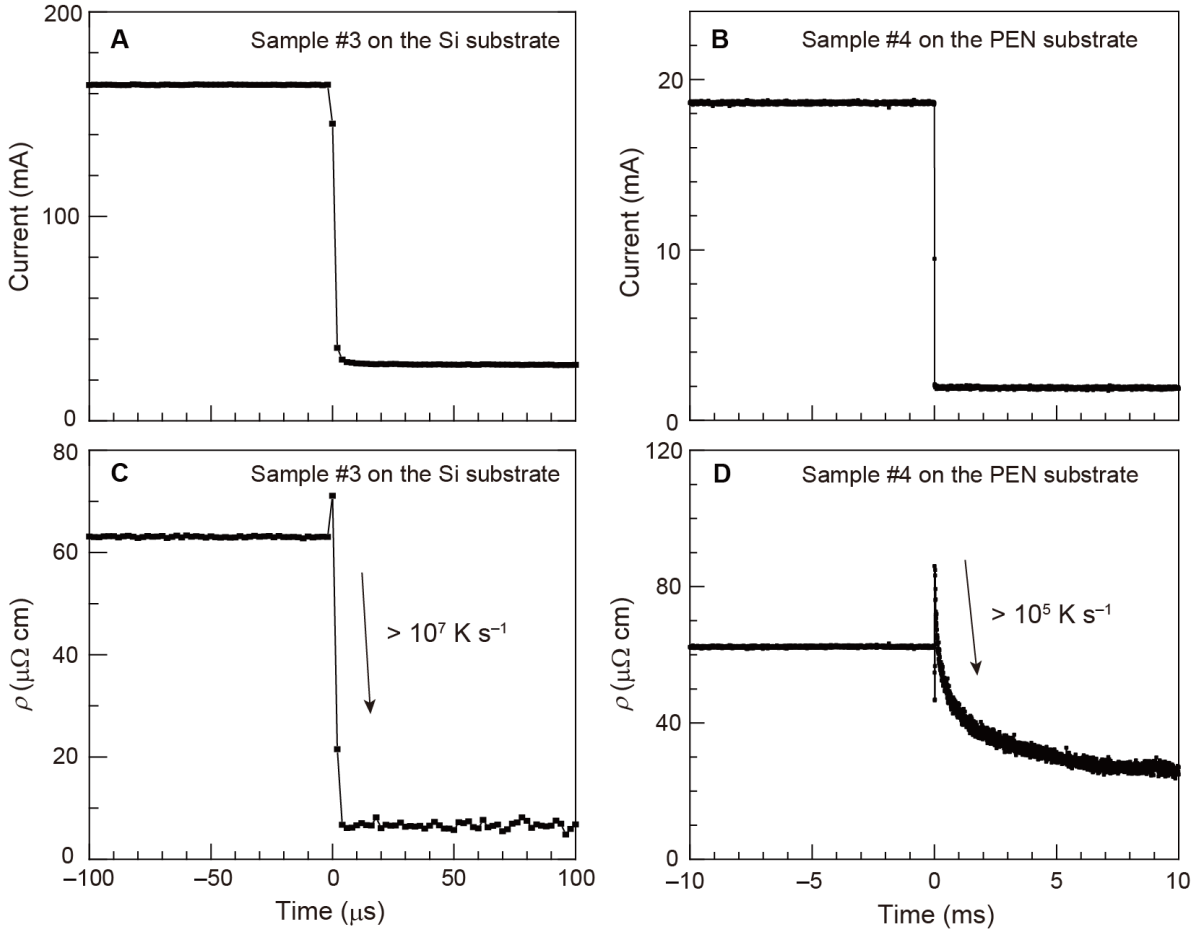

Fig. S2. Measurements of the highest quenching rate achieved in the present experiments. (**A** to **D**) The time profiles of the current applied to the $IrTe_2$ thin plate #3 ($V \approx 18$ μm^3) on the Si substrate (A) and #4 ($V \approx 180$ μm^3) on the PEN substrate (B) and the corresponding change in resistivity for sample #3 (C) and #4 (D). The origin of the time is set at the beginning of the pulse fall. From the time-resistivity profiles, the order of magnitudes of the achieved quenching rate is estimated as shown in (C) and (D).

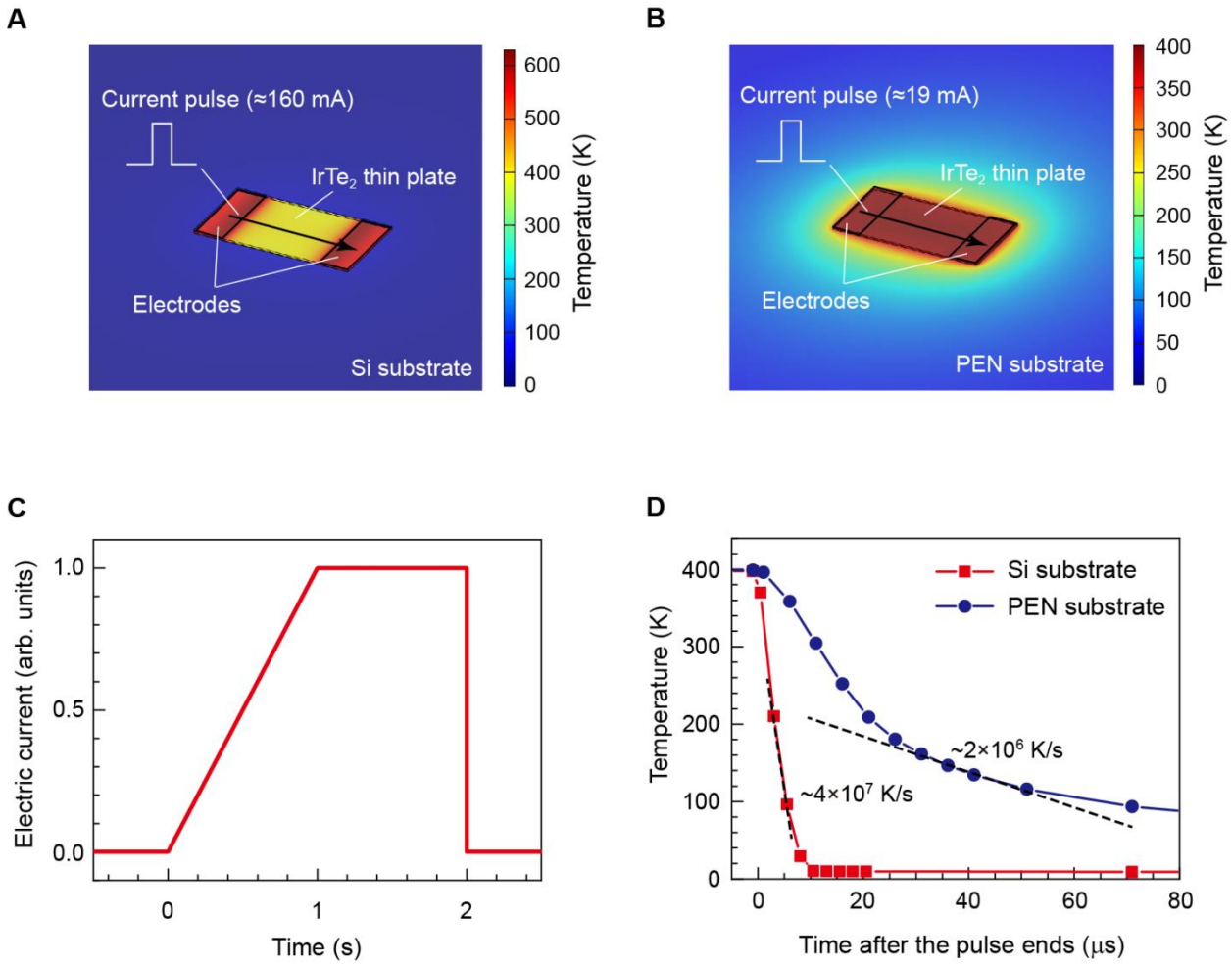

Fig. S3. Simulation results of the quenching process for an $IrTe_2$ thin plate on Si and PEN substrates. (**A** and **B**) The spatial distribution of temperature during the pulse top for a $IrTe_2$ thin plate on Si substrate (A) and that on a PEN substrate (B). Before the pulse application, the sample and substrate are in equilibrium at 4 K. (**C**) The time profile of the current amplitude used in the simulations. The value of the pulse top is 160 and 19 mA for a thin plate on the Si and PEN substrates, respectively. (**D**) The time profiles of the sample temperature during the quenching following the pulse application. The average cooling rates in 100–200 K are estimated from the profiles.

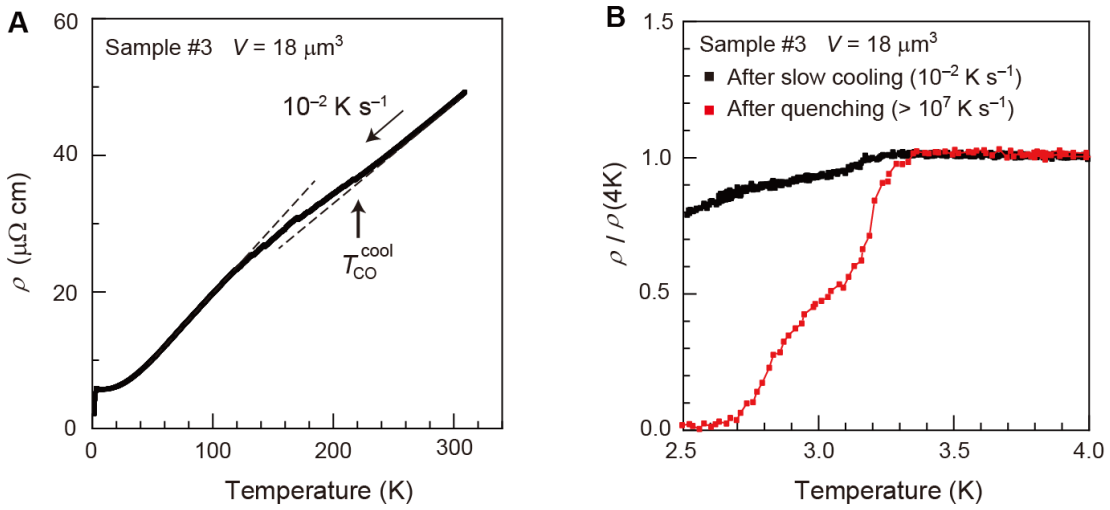

Fig. S4. Creation of persistent superconductivity by a current application in the $IrTe_2$ thin plate #3. (**A**) The temperature-resistivity profile measured at a cooling rate of 10^{-2} K s^{-1}. A weak resistivity anomaly accompanying the charge order is observed, the onset of which is indicated by the arrow. (**B**) The temperature-resistivity profiles at low temperatures after slow cooling and quenching to 4 K.

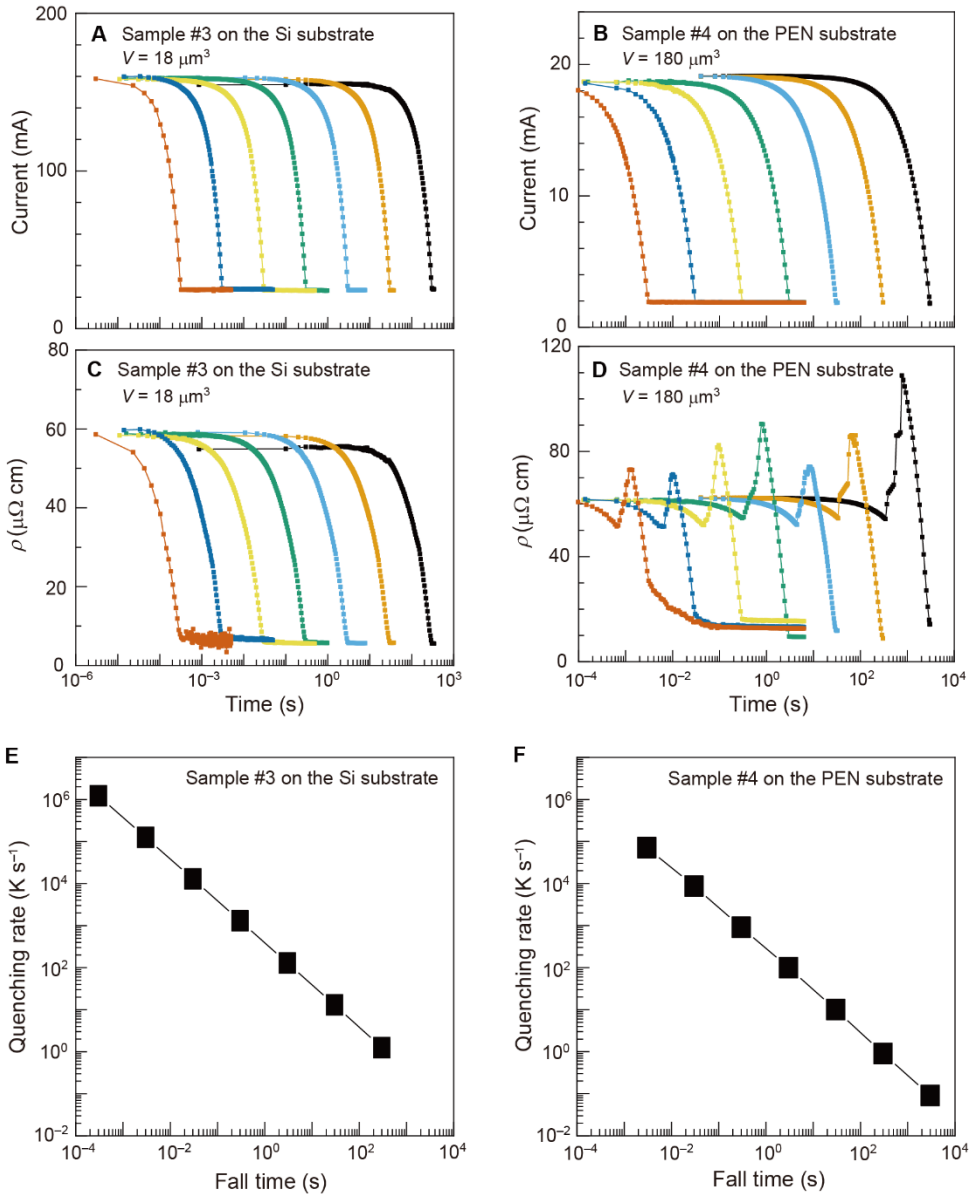

Fig. S5. Manipulation of the quenching rate by controlling the pulse fall time. (**A** to **D**) The time profiles of the current applied to the $IrTe_2$ thin plate #3 on the Si substrate (A) and #4 on the PEN substrate (B), as well as the corresponding change in resistivity for #3 (C) and #4 (D). The time profiles displayed in (C) and (D) were recorded under the current profile with the corresponding color in (A) and (B), respectively. The origin of the time is set at the beginning of the pulse fall. (**E** and **F**) Estimated quenching rate at each fall time for thin plates #3 (E) and #4 (F).

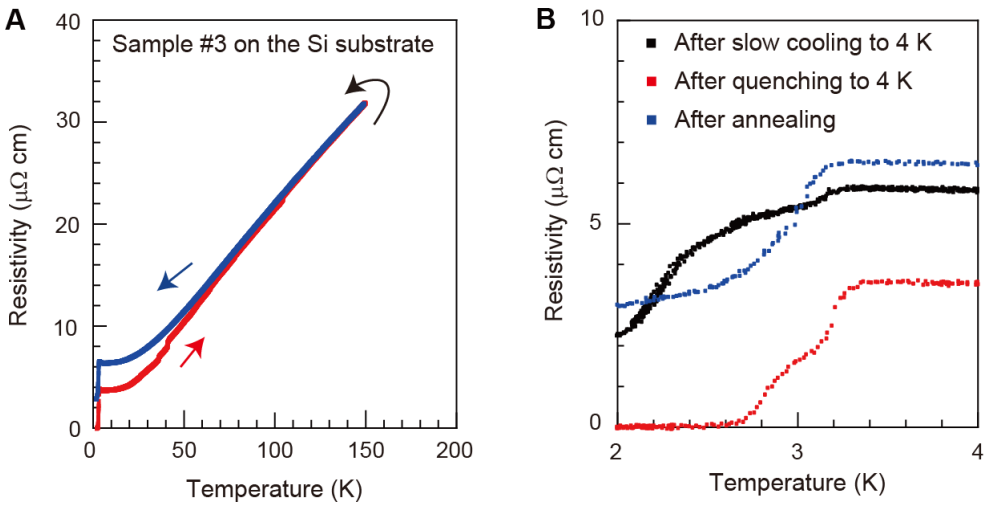

Fig. S6. Annealing process of the quenched metastable state in the $IrTe_2$ thin plate #3 on the Si substrate. (**A**) The temperature-resistivity profile upon heating from 2 to 150 K at a rate of 3×10^{-3} K s^{-1} (the red curve) and subsequent cooling to 2 K at a rate of 10^{-2} K s^{-1} (the blue curve). Above 50 K, the red and blue curves exhibit quantitatively similar behaviors, indicating that the quenched metastable state is thermally annealed and thus relaxed into the slowly cooled state. (**B**) The temperature-resistivity profiles at low temperatures after slow cooling or quenching to 4 K and after the annealing process. The applied quenching rate is $>10^{7}$ K s^{-1}.

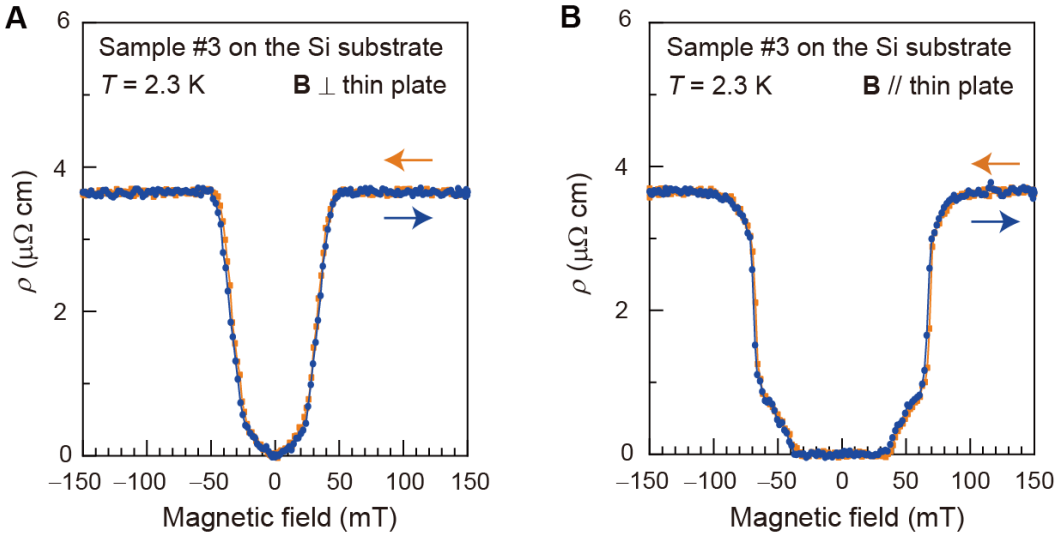

Fig. S7. Magnetic field effects on the emergent superconductivity in the quenched metastable states. (**A** and **B**) The magnetic-field dependence of the resistivity with the field direction perpendicular (A) and parallel (B) to the $IrTe_2$ thin plate #3.